Energy stable and linearly well-balanced numerical schemes for the non-linear Shallow Water equations with Coriolis force

Emmanuel Audusse, Virgile Dubos, Noémie Gaveau, Yohan Penel

Energy stable and linearly well-balanced numerical schemes for the non-linear Shallow Water equations with Coriolis force

Emmanuel Audusse * Virgile Dubos † Noémie Gaveau ‡ Yohan Penel §

January 4, 2022

Abstract

This work is dedicated to the analysis of a class of energy stable and linearly well-balanced numerical schemes dedicated to the non-linear Shallow Water equations with Coriolis force. The proposed algorithms rely on colocated finite volume approximations formulated on cartesian geometries. They involve appropriate diffusion terms in the numerical fluxes, expressed as discrete versions of the linear geostrophic equilibrium. We show that the resulting methods ensure semi-discrete energy estimates and numerical results show a very clear improvement around the nonlinear geostrophic equilibrium when compared to those of classic Godunov-type schemes.

1 Introduction

The question of the accuracy of numerical schemes for hyperbolic systems with source terms around stationary solutions and/or in asymptotic regimes has been a subject of great interest over the last two decades, see the seminal works [4,14,15] in late nineties and the reference books [6,13] ten years later. In the context of geophysical flows and for colocated finite-volume methods applied to shallow water equations, a lot of works have been devoted to the accuracy around the so-called lake-at-rest equilibrium and more recently extended to nonzero velocity one dimensional stationary states, see [5] and references therein. But for large scales atmospheric or oceanographic flows, the relevant stationary state is the geostrophic equilibrium, see [27] for a general introduction to geophysical rotating fluid dynamics. The accuracy of colocated finite volume numerical schemes around such an equilibrium was less investigated, To our knowledge, the first work in this field is due to Bouchut, Le Sommer and Zeitlin [7], see also [8] and [9], but was fully accurate only for one-dimensional flows, as exhibited in [1]. Recently two independent works [19,26] proposed IMplicit-EXplicit type schemes for fully nonlinear equations which are proved to be accurate near the geostrophic equilibrium but, due to their implicit part, need the solution of a global Laplacian at each time step, see also [25] for a study about the time discretization of the Coriolis term. Note that there exists also a lot of works devoted to the approximation of the Coriolis term in staggered schemes, see for example [22] for a linear analysis and [21] for the fully nonlinear case. Let us also mention the work [24] where the authors compare the dispersion relations of some mixed Finite Volume / Finite Difference and Finite Volume / Finite Element methods in a large scale oceanographic context including the Coriolis force.

In this work, we aim at designing explicit colocated finite volume schemes that are proved to be accurate around the geostrophic equilibrium and stable in the nonlinear framework. Our work is based on the ideas developed in [1] where accurate and stable Godunov type schemes were designed for the linear two-dimensional rotating wave equation but we will see in the sequel that further developments are needed to take charge of the non linear case in a conservative way. All the numerical finite volume scheme we consider in this paper belong to the AUSM family where the flux is divided in an advective part and a pressure part, see the seminal works [18] and [17] and the recent review [11]. More precisely, in Section 2, we first introduce the system of equations and we characterize the geostrophic equilibrium. In Section 3, we define some discrete operators and we prove some of their properties. Equipped with these definitions, in Section 4, we can define some finite volume schemes and study the two properties we are interested in : the decrease of the semi-discrete energy and the preservation of the geostrophic equilibrium in the linearized version. Note that all along the paper the term semi-discrete will refer to quantities that are discrete

*LAGA, Institut Galilée, Université Sorbonne Paris Nord – 99 avenue Jean-Baptiste Clément, 93430 Villetaneuse.
†Laboratoire d'hydraulique Saint-Venant, École des Ponts, EDF'lab Chatou – 6 quai Wattier, 78401 Chatou.
‡Institut Denis Poisson, Université D'Orléans, rue de Chartres, 45067 Orléans.
§INRIA Paris – Sorbonne Université – CNRS (LJLL), team ANGE, 2 rue Simone Iff, CS 42112, 75589 Paris cedex 12.

in space but continuous in time. Finally, in Section 5, we illustrate the behaviour of the schemes for some standard test cases and we exhibit a great improvement when compared to a classical finite volume scheme.

2 Shallow water equations and geostrophic equilibrium

Let Ω be an open bounded domain of $\mathbb{R}^2$ and let $T > 0$. The nonlinear Shallow Water equations with Coriolis force formulated on $\Omega \times (0, T)$ read:

$$\begin{cases} \partial_t h + \operatorname{div}(h\boldsymbol{u}) = 0\,, \\ \partial_t (h\boldsymbol{u}) + \operatorname{div}(h\boldsymbol{u} \otimes \boldsymbol{u}) + h(\nabla\phi + \omega \boldsymbol{u}^\perp) = 0\,, \end{cases} \tag{1}$$

where h is the water height and $\boldsymbol{u} = (u_x, u_y)$ the horizontal velocity, $\boldsymbol{u}^\perp = (-u_y, u_x)$ denoting its orthogonal vector in the (x, y) plane. The Coriolis force is accounted for in the momentum equations through the angular speed ω. Following [10, 20], the pressure forces appear under a non conservative form through the scalar potential $\phi = gh$, where g is the standard gravity constant. For the sake of simplicity, a flat topography is considered in the present work, but the proposed approaches naturally extended to varying bottoms by taking $\phi = g(h + b)$ where b denotes the topography. It is also easy to extend the method to a varying Coriolis parameter in the β-plane approximation since all the modifications we introduce in this paper are purely local.

It is well-known that the total energy associated to the system (1) decomposes as $E = \mathcal{P} + \mathcal{K}$ where

$$\mathcal{P} = \frac{1}{2} g h^2 \quad \text{and} \quad \mathcal{K} = \frac{1}{2} h \|\boldsymbol{u}\|^2$$

stand respectively for potential and kinetic energies. We recall that the energy E plays the role of a mathematical entropy associated to the hyperbolic system (1) and regular solutions satisfy the following conservation law

$$\partial_t E + \operatorname{div}\left[\left(\phi + \frac{1}{2}\|\boldsymbol{u}\|^2\right) h\boldsymbol{u}\right] = 0\,. \tag{2}$$

whereas for discontinuous solution, the total energy is only non-increasing in time. When developing numerical methods, main objectives are accuracy and stability. To get stability, a crucial objective is to build numerical approximations satisfying a discrete counterpart of (2) that ensures that the discrete energy is nonincreasing. To achieve this, a general strategy is to consider a sufficient amount of numerical diffusion in the scheme. But in some physical contexts such as low Froude number regimes or near specific stationary states, these diffusive terms may considerably degrade the accuracy of the approximations and specific schemes are needed. Here we are interested in flows around the geostrophic balance :

$$\nabla\phi + \omega \boldsymbol{u}^\perp = 0\,, \quad \operatorname{div} \boldsymbol{u} = 0 \tag{3}$$

To address such an issue, based on the study for the linear case [1], we propose a numerical approach involving discrete versions of these equilibria in the numerical fluxes. As a preliminary step, the strategy can be understood at the continuous level by investigating how the model (1) behaves with respect to some generic perturbations $(\boldsymbol{q}, \pi)$:

$$\begin{cases} \partial_t h + \operatorname{div}(h\boldsymbol{u} - \boldsymbol{q}) = 0\,, \\ \partial_t (h\boldsymbol{u}) + \operatorname{div}\left(\boldsymbol{u} \otimes (h\boldsymbol{u} - \boldsymbol{q})\right) + (h\nabla\phi - \nabla\pi) + \omega\,(h\boldsymbol{u} - \boldsymbol{q})^\perp = 0\,, \end{cases} \tag{4}$$

where $\boldsymbol{q}$ and π can be respectively seen as (small) perturbations with respect to the flow rate and to the hydrostatic pressure. The solutions to the modified equations (4) satisfy the following energy balance:

$$\partial_t E + \operatorname{div}\left[\left(\phi + \frac{1}{2}\|\boldsymbol{u}\|^2\right)\ (h\boldsymbol{u} - \boldsymbol{q}) - \pi\boldsymbol{u}\right] = -\boldsymbol{q} \cdot \left(\nabla\phi + \omega\boldsymbol{u}^\perp\right) - \pi\ \operatorname{div} \boldsymbol{u}\,, \tag{5}$$

which motivates a choice for $\boldsymbol{q}$ and π involving resp. the quantities $\nabla\phi + \omega\,\boldsymbol{u}^\perp$ and $\operatorname{div} \boldsymbol{u}$. Let us remark that these quantities govern the geostrophic equilibrium (3) associated to System (1) linearized around the steady state $(\tilde{h}, \widetilde{\boldsymbol{u}}) = (h_0, 0)$ for a constant h_0:

$$\begin{cases} \partial_t h = -h_0\ \operatorname{div} \boldsymbol{u}\,, \\ \partial_t \boldsymbol{u} = -(\nabla\phi + \omega\,\boldsymbol{u}^\perp)\,. \end{cases}$$

From a numerical point of view, diffusion terms are thus expected to have regularizing effects in the sense that they allow to recover a discrete counterpart of (5). Moreover, such terms are intended to vanish close to the geostrophic equilibrium, which must improve the quality of the approximations in this regime. The rest of the article is then devoted to the presentation of different ways to implement this idea in a discrete setting.

3 Discrete operators

3.1 Definition of the mesh

Let us first introduce some generic notations related to the discretization of the equations. We consider a uniform tessellation $\mathbb{T}$ of the computational domain $\Omega \subset \mathbb{R}^2$ made of non-overlapping rectangular cells of sizes Δx, Δy. The set of all edges of the mesh is denoted by $\mathcal{E}$ and the set of vertices by $\mathbb{V}$.

- A generic cell of $\mathbb{T}$ is denoted by K and its boundary by ∂K. A given quantity Φ located on K is numbered $\Phi_{i,j}$.
- A generic edge of $\mathcal{E}$ is denoted by e and its length by m_e. A given quantity Φ located on e is numbered $\Phi_{i+1/2,j}$ (respectively $\Phi_{i,j+1/2}$) for y-axis (respectively x-axis) edge.
- Given a cell K and an edge $e \in \partial K$, K_e is the neighbouring cell to e (other than K) and $\boldsymbol{n}_{e,K}$ the outward normal pointing to K_e.
- A generic vertex of $\mathbb{V}$ is denoted by v. A given quantity Φ located on v is numbered $\Phi_{i+1/2,j+1/2}$.

Notations are pictured on Figs. 1.

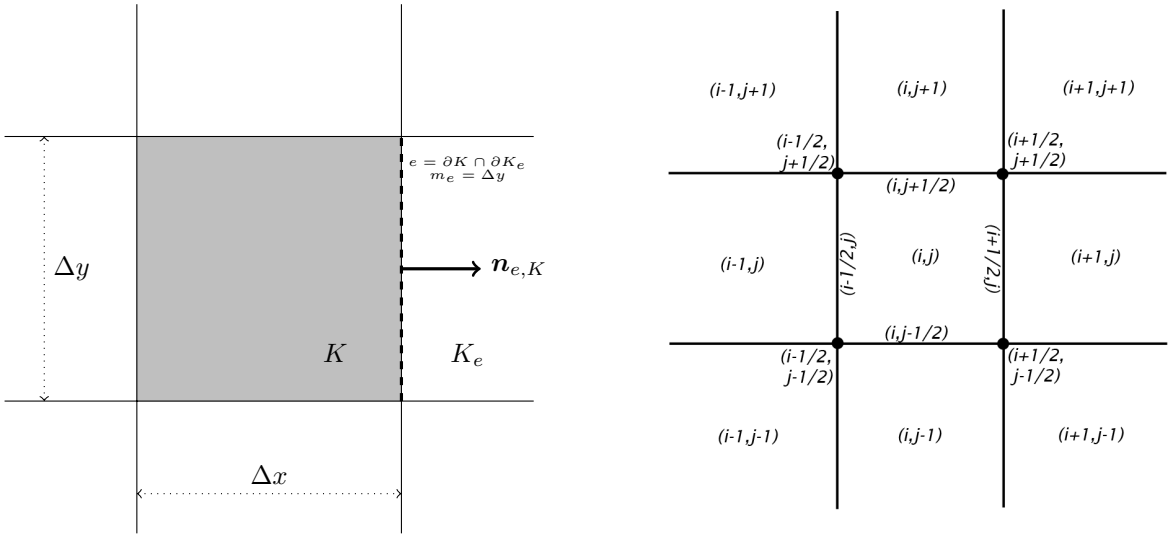

(a) Mesh notations

(b) Variables numbering

Figure 1: Geometric notations

3.2 Discrete operators

Equipped with these geometrical settings, we can now introduce discrete operators that will be needed to construct numerical schemes. Since we only consider colocated finite volume schemes, all the unknowns are defined on the cells $K \in \mathbb{T}$. But we will see in the next sections that some other quantities (including the numerical diffusion terms) need to be computed on the edges $e \in \mathcal{E}$ or at the vertices $v \in \mathbb{V}$. Then we need to define discrete operators from cells to edges (and vice-versa) and from cells to vertices (and vice-versa) – see Figure 1. In the following definitions, the notations $X_i^j(\phi_j)$ means that the operator X is applied to a quantity ϕ defined at the location j and

computes a quantity that is defined at the location i. For example, the first operator below $\nabla_e^K \varphi_K$ is a discrete gradient operator that is defined for quantities that are defined on a cell K and that allows to construct a consistent gradient on an edge e. Discrete gradient and divergence are denoted with classical notations. The notation f always denotes an algebraic reconstruction operator. Let us begin with the operators from cells to edges (and vice-versa).

$$\nabla_e^K \varphi_K = \frac{m_e}{\Delta x \Delta y}(\varphi_{Ke} - \varphi_K)\ \boldsymbol{n}_{e,K} \qquad \mathrm{div}_K^e\, \boldsymbol{\varphi_e} = \frac{1}{\Delta x \Delta y} \sum_{e \subset \partial K} m_e\, \boldsymbol{\varphi}_e \cdot \boldsymbol{n}_{e,K}$$

$$f_e^K(\boldsymbol{\varphi}_K) = \frac{1}{2}(\boldsymbol{\varphi}_{Ke} + \boldsymbol{\varphi}_K) \cdot \boldsymbol{n}_{e,K}\ \boldsymbol{n}_{e,K} \qquad f_K^e(\boldsymbol{\varphi}_e) = \frac{1}{2} \sum_{e \subset \partial K} \boldsymbol{\varphi}_e \cdot \boldsymbol{n}_{e,K}\ \boldsymbol{n}_{e,K}$$

Then we define operators from cells to vertices, where we use the notation $\boldsymbol{\varphi} = (\varphi, \psi)$

$$[\nabla_v^K \varphi_K]_{i+1/2,j+1/2} = \frac{1}{2} \begin{pmatrix} \dfrac{\varphi_{i+1,j+1} - \varphi_{i,j+1}}{\Delta x} + \dfrac{\varphi_{i+1,j} - \varphi_{i,j}}{\Delta x} \\ \dfrac{\varphi_{i+1,j+1} - \varphi_{i+1,j}}{\Delta y} + \dfrac{\varphi_{i,j+1} - \varphi_{i,j}}{\Delta y} \end{pmatrix}$$

$$[\mathrm{div}_v^K\, \boldsymbol{\varphi}_K]_{i+1/2,j+1/2} = \frac{1}{2}\left[\frac{\varphi_{i+1,j+1} - \varphi_{i,j+1}}{\Delta x} + \frac{\varphi_{i+1,j} - \varphi_{i,j}}{\Delta x}\right] + \frac{1}{2}\left[\frac{\psi_{i+1,j+1} - \psi_{i+1,j}}{\Delta y} + \frac{\psi_{i,j+1} - \psi_{i,j}}{\Delta y}\right]$$

$$[f_v^K(\boldsymbol{\varphi}_K)]_{i+1/2,j+1/2} = \frac{\boldsymbol{\varphi}_{i+1,j+1} + \boldsymbol{\varphi}_{i,j+1} + \boldsymbol{\varphi}_{i+1,j} + \boldsymbol{\varphi}_{i,j}}{4}$$

and from vertices to cells

$$[\nabla_K^v \varphi_v]_{i,j} = \frac{1}{2} \begin{pmatrix} \dfrac{\varphi_{i+1/2,j+1/2} - \varphi_{i-1/2,j+1/2}}{\Delta x} + \dfrac{\varphi_{i+1/2,j-1/2} - \varphi_{i-1/2,j-1/2}}{\Delta x} \\ \dfrac{\varphi_{i+1/2,j+1/2} - \varphi_{i+1/2,j-1/2}}{\Delta y} + \dfrac{\varphi_{i-1/2,j+1/2} - \varphi_{i-1/2,j-1/2}}{\Delta y} \end{pmatrix}$$

$$\begin{aligned}[\mathrm{div}_K^v\, \boldsymbol{\varphi}_v]_{i,j} = {} & \frac{1}{2}\left[\frac{\varphi_{i+1/2,j+1/2} - \varphi_{i-1/2,j+1/2}}{\Delta x} + \frac{\varphi_{i+1/2,j-1/2} - \varphi_{i-1/2,j-1/2}}{\Delta x}\right] \\ & + \frac{1}{2}\left[\frac{\psi_{i+1/2,j+1/2} - \psi_{i+1/2,j-1/2}}{\Delta y} + \frac{\psi_{i-1/2,j+1/2} - \psi_{i-1/2,j-1/2}}{\Delta y}\right]\end{aligned}$$

$$[f_K^v(\boldsymbol{\varphi}_v)]_{i,j} = \frac{\boldsymbol{\varphi}_{i+1/2,j+1/2} + \boldsymbol{\varphi}_{i-1/2,j+1/2} + \boldsymbol{\varphi}_{i+1/2,j-1/2} + \boldsymbol{\varphi}_{i-1/2,j-1/2}}{4}$$

We will also need a divergence operator from edges to vertices:

$$[\mathrm{div}_v^e\, \boldsymbol{\Phi}_e]_{i+1/2,j+1/2} = \frac{1}{\Delta x}\left(\boldsymbol{\Phi}_{i+1,j+1/2} - \boldsymbol{\Phi}_{i,j+1/2}\right) \cdot \boldsymbol{e}_x + \frac{1}{\Delta y}\left(\boldsymbol{\Phi}_{i+1/2,j+1} - \boldsymbol{\Phi}_{i+1/2,j}\right) \cdot \boldsymbol{e}_y,$$

a reconstruction operator from from edges to vertices:

$$f_v^e(\boldsymbol{\varphi}_e) = \frac{1}{2} \sum_{e \in \mathcal{E}(v)} \boldsymbol{\varphi}_e$$

with $\mathcal{E}(v) = \{e \in \mathcal{E} \mid v \in e\}$ the set of adjacent edges to vertex v and a reconstruction operator from vertices to edges:

$$f_e^v(\boldsymbol{\varphi}_v) = \frac{1}{2} \sum_{v \in \partial e} \boldsymbol{\varphi}_v \cdot \boldsymbol{n}_{e,K}\ \boldsymbol{n}_{e,K}.$$

Finally we need to define upwind divergence operators that will be used to discretize the transport part of the equations in order to ensure the stability of the numerical schemes. In the following definitions, the quantity

$$\varphi^{\pm} = \frac{1}{2}(\varphi \pm |\varphi|)$$

will refer to the positive and negative parts of any scalar function φ. From edges to cells, the operator reads

$$\mathbf{div}_K^{e,up}(\boldsymbol{\psi}_K \otimes \boldsymbol{\varphi}_e) = \frac{1}{\Delta x \Delta y} \sum_{e \subset \partial K} m_e \left(\boldsymbol{\psi}_K (\boldsymbol{\varphi}_e \cdot \boldsymbol{n}_{e,K})^+ + \boldsymbol{\psi}_{K_e} (\boldsymbol{\varphi}_e \cdot \boldsymbol{n}_{e,K})^-\right)$$

3.3 Mimetic properties

These discrete operators satisfy some important properties that will be used to prove some results for the numerical schemes we propose in the next section.

Lemma 3.1. *We first mention some local properties about the permutation of the derivative, reconstruction and orthogonal operators. Computations are obvious.*

i) $f_v^K(\boldsymbol{u}_K^\perp) = (f_v^K\,\boldsymbol{u}_K)^\perp$

ii) $-\operatorname{div}_v^e((f_e^K(\boldsymbol{u}_K^\perp))^\perp) = \operatorname{div}_v^K\,\boldsymbol{u}_K$

iii) $\operatorname{div}_K^v(f_v^K\,\boldsymbol{u}_K) = f_K^v(\operatorname{div}_v^K\,\boldsymbol{u}_K)$

iv) $\operatorname{div}_K^v(f_v^K(h_K\boldsymbol{u}_K)) = \operatorname{div}_K^e(f_e^v(f_v^K(h_K\boldsymbol{u}_K)))$

We now define the three scalar products

$$\langle \boldsymbol{\Phi}_K, \boldsymbol{\Psi}_K\rangle = \sum_{K\in\mathbb{T}} \boldsymbol{\Phi}_K\cdot\boldsymbol{\Psi}_K, \quad \langle \boldsymbol{\Phi}_v, \boldsymbol{\Psi}_v\rangle = \sum_{v\in\mathbb{V}} \boldsymbol{\Phi}_v\cdot\boldsymbol{\Psi}_v$$

$$\text{and}\quad \langle \boldsymbol{\varphi}_e, \boldsymbol{\Psi}_e\rangle = \sum_{i,j}\left[(\boldsymbol{\varphi}_{i+1/2,j}\cdot\boldsymbol{e}_x)(\boldsymbol{\Psi}_{i+1/2,j}\cdot\boldsymbol{e}_x) + (\boldsymbol{\varphi}_{i,j+1/2}\cdot\boldsymbol{e}_y)(\boldsymbol{\Psi}_{i,j+1/2}\cdot\boldsymbol{e}_y)\right].$$

Lemma 3.2. *We have the following properties for the reconstruction and orthogonal operators*

i) $\langle \boldsymbol{u}_K, (f_K^e\,\boldsymbol{q}_e)^\perp\rangle = -\langle f_e^K(\boldsymbol{u}_K^\perp), \boldsymbol{q}_e\rangle$

ii) $\langle f_K^v(f_v^K(\boldsymbol{u}_K^\perp)), \boldsymbol{u}_K\rangle = 0$

Proof. Property i) is obtained after a rearrangement of sum under the condition $\boldsymbol{q}_e = 0$ on the edges on the boundary of the physical domain to eliminate the boundary terms.
Property ii) is obtained after a rearrangement of sum under the periodic boundary conditions on h_K and $\boldsymbol{u}_K$ to eliminate the boundary terms. □

Lemma 3.3. *We have the following mimetic properties for the discrete gradient and divergence operators, including for some of them the reconstruction operators*

i) $\langle \phi_K, \operatorname{div}_K^e\,\boldsymbol{q}_e\rangle = -\langle \nabla_e^K\,\phi_K, \boldsymbol{q}_e\rangle$

ii) $\langle \pi_v, \operatorname{div}_v^K\,\boldsymbol{u}_K\rangle = -\langle \nabla_K^v\,\pi_v, \boldsymbol{u}_K\rangle$

iii) $\langle f_K^e(\nabla_e^K\,\phi_K), h_K\boldsymbol{u}_K\rangle = -\langle \phi_K, \operatorname{div}_K^e(f_e^K(h_K\boldsymbol{u}_K))\rangle$

iv) $\langle f_K^v(\nabla_v^K\,\phi_K), \boldsymbol{u}_K\rangle = -\langle \phi_K, f_K^v(\operatorname{div}_v^K\,\boldsymbol{u}_K)\rangle$

Proof. Property i) (respectively ii)) is obtained after a rearrangement of sum under the condition $\boldsymbol{q}_e = 0$ on the edges (respectively $\pi_v = 0$ on the vertices) on the boundary of the physical domain to eliminate the boundary terms.
Property iii) and iv) are obtained after a rearrangement of sum under the periodic boundary conditions on h_K and $\boldsymbol{u}_K$ to eliminate the boundary terms. □

4 Well-balanced and stable finite volume schemes

When considering hyperbolic equations, classical finite volume schemes in colocated two-dimensional cartesian framework are often referred as five points schemes. Indeed the update of the quantities of interest in a cell K of the tesselation $\mathbb{T}$ needs the computation of the fluxes through the four edges of its boundary ∂K, see Figure 1. For a first order scheme, the numerical flux through an edge $e \in \mathcal{E}$ is generally computed from the values of the quantities in the two neighbouring cells. Hence, the update of the quantities in a cell K involves five cells of the tesselation $\mathbb{T}$. We refer to [16, 23] for more details about classical first order finite volume schemes for hyperbolic problems.

In the last section of the paper, devoted to the numerical tests, such a five point scheme, typically the HLLC scheme, see [23], will be considered as a standard scheme to which we will compare the well-balanced schemes we designed in the next sections. Because of the fundamentally two-dimensional character of the geostrophic equilibrium, these well-balanced schemes have to involve a larger stencil. Note that to consider enlarged stencils is also a common way to design high order schemes in a finite volume framework through the MUSCL strategy, see [16, 23], and is also commonly used in diffusion problems since the computation of the numerical flux needs the reconstruction of a complete two-dimensional gradient, see [12].

In this section, we present different nine points schemes for the shallow water equations with Coriolis source term, based on a discretization of the geostrophic equilibrium (3) on the edges.

4.1 Entropic well-balanced scheme

Considering the operators defined in section 3.2 we can see the discretization of the geostrophic equilibrium (3) on the vertices as a reconstruction of its discretization on the edges. Thus, in this section we define a nine points mixed scheme in which the geostrophic equilibrium is reconstructed sometimes on the vertices and sometimes on the edges. The perturbation q, see (4), is defined at the edges e whereas the perturbation π is defined on the vertices v. The scheme ensure both the preservation of the linearized stationary states and the decreasing of the nonlinear semi-discrete energy and we thus will later refer to as the "entropic well-balanced scheme". Theoretically, the scheme presents spurious solutions on the velocity, however the numerical results presented in the last section of the paper exhibit a reasonably good behaviour for all the test cases we have performed.

$$\begin{cases} \dfrac{\mathrm{d}}{\mathrm{dt}} h_K + \mathrm{div}_K^e(\boldsymbol{\mathcal{F}}_e) = 0, \\ \dfrac{\mathrm{d}}{\mathrm{dt}}(h_K \boldsymbol{u}_K) + \mathbf{div}_K^{e,up}(\boldsymbol{u}_K \otimes \boldsymbol{\mathcal{F}}_e) + h_K\, f_K^v(\,\nabla_v^K\,\phi_K) - \nabla_K^v\,\pi_v = -\omega\left(h_K\, f_K^v(f_v^K\,\boldsymbol{u}_K) - f_K^e\,\boldsymbol{q}_e\right)^\perp, \end{cases} \tag{6}$$

where the interface fluxes are defined at the level of the edge e as:

$$\boldsymbol{\mathcal{F}}_e = f_e^v(f_v^K(h_K \boldsymbol{u}_K)) - \boldsymbol{q}_e\,, \tag{7}$$

with the numerical diffusion term on the flow rate

$$\boldsymbol{q}_e = \gamma\,\frac{\Lambda}{g}\,\max\{\Delta x, \Delta y\}(\omega\, f_e^K(\boldsymbol{u}_K^\perp) + \nabla_e^K\,\phi_K), \tag{8}$$

while the numerical diffusion term on the hydrostatic pressure is defined at the vertices

$$\pi_v = \nu\Lambda\ \max\{\Delta x, \Delta y\}\, f_v^K(h_K)\,\mathrm{div}_v^K\,\boldsymbol{u}_K, \tag{9}$$

where γ and ν are positive dimensionless constants, and Λ is a positive characteristic velocity. Typically, we take

$$\Lambda = \max_{K\in\mathbb{T}}\left\{\|\boldsymbol{u}_K\| + \sqrt{g h_K}\right\}.$$

Semi-discrete energy : We first show the scheme (6) ensures a discrete counterpart of (5) through semi-discrete mechanic energy estimates. We need the two following lemmas, describing the evolution of potential and kinetic energies.

Lemma 4.1 (Potential energy)**.** *We set* $\mathcal{P}_K = \dfrac{1}{2} g\,(h_K)^2$ *for* $K \in \mathbb{T}$*. Then:*

$$\frac{\mathrm{d}}{\mathrm{dt}}\mathcal{P}_K + \phi_K\,\mathrm{div}_K^v(f_v^K(h_K \boldsymbol{u}_K)) - \phi_K\,\mathrm{div}_K^e\,\boldsymbol{q}_e = 0. \tag{10}$$

Proof. Property iv) of lemma 3.1. □

Lemma 4.2 (Kinetic energy)**.** *We set* $\mathcal{K}_K = \dfrac{1}{2} h_K \|\boldsymbol{u}_K\|^2$ *for* $K \in \mathbb{T}$*. Then:*

$$\begin{aligned} \frac{\mathrm{d}}{\mathrm{dt}}\mathcal{K}_K + \frac{1}{2}\,\mathbf{div}_K^{e,up}\left(\|\boldsymbol{u}_K\|^2 \boldsymbol{\mathcal{F}}_e\right) + h_K \boldsymbol{u}_K \cdot f_K^v\left(\nabla_v^K\,\phi_K\right) \\ \leq -\omega\left(h_K \boldsymbol{u}_K \cdot f_K^v(f_v^K(\boldsymbol{u}_K^\perp)) - \boldsymbol{u}_K \cdot (f_K^e\,\boldsymbol{q}_e)^\perp\right) + \boldsymbol{u}_K \cdot \nabla_K^v\,\pi_v). \end{aligned} \tag{11}$$

Proof. Using the first equation of (6) we write:

$$\begin{aligned}\frac{\mathrm{d}}{\mathrm{dt}}\left(\frac{1}{2}h_K\|\boldsymbol{u}_K\|^2\right) &= \boldsymbol{u}_K\cdot\frac{\mathrm{d}}{\mathrm{dt}}(h_K\boldsymbol{u}_K)-\frac{1}{2}\|\boldsymbol{u}_K\|^2\frac{\mathrm{d}}{\mathrm{dt}}h_K\\ &= -h_K\boldsymbol{u}_K\cdot f_K^v(\nabla_v^K\,\phi_K)-\boldsymbol{u}_K\cdot\mathbf{div}_K^{e,up}(\boldsymbol{u}_K\otimes\boldsymbol{\mathcal{F}}_e)+\omega\boldsymbol{u}_K\cdot(f_K^e\,\boldsymbol{q}_e)^\perp\\ &\quad+\frac{1}{2}\|\boldsymbol{u}_K\|^2\,\mathrm{div}_K^e\,\boldsymbol{\mathcal{F}}_e+\boldsymbol{u}_K\cdot\nabla_K^v\,\pi_v\,-\omega h_K\boldsymbol{u}_K\,f_K^v(f_v^K(\boldsymbol{u}_K^\perp)).\end{aligned}$$

After some basic computations, we get the relations

$$\begin{aligned}&\frac{1}{2}\|\boldsymbol{u}_K\|^2\,\mathrm{div}_K^e\,\boldsymbol{\mathcal{F}}_e-\boldsymbol{u}_K\cdot\mathbf{div}_K^{e,up}\,(\boldsymbol{u}_K\otimes\boldsymbol{\mathcal{F}}_e)\\ &\qquad=-\frac{1}{2}\,\mathbf{div}_K^{e,up}\left(\|\boldsymbol{u}_K\|^2\boldsymbol{\mathcal{F}}_e\right)+\frac{1}{2\Delta x\Delta y}\sum_{e\subset\partial K}m_e\|\boldsymbol{u}_K-\boldsymbol{u}_{Ke}\|^2\left(\boldsymbol{\mathcal{F}}_e\cdot\boldsymbol{n}_{e,k}\right)^-\,. \quad (12)\end{aligned}$$

The second term of the right hand side being non-positive, we get the announced result . □

Proposition 4.3 (Decreasing of the semi-discrete energy)**.** *We define the total energy $E_K=\mathcal{P}_K+\mathcal{K}_K$. Then we obtain a discrete counterpart of* (5)

$$\begin{aligned}&\frac{\mathrm{d}}{\mathrm{dt}}\left(\sum_{K\in\mathbb{T}}\Delta x\Delta y E_K\right)\\ &\qquad\le-\Delta x\Delta y\max\{\Delta x,\Delta y\}\left[\sum_{v\in\mathbb{V}}\left[\nu\Lambda\,f_v^K(h_K)(\mathrm{div}_v^K\,\boldsymbol{u}_K)^2\right]+\sum_{e\in\mathbb{E}}\left[\gamma\,\frac{\Lambda}{g}\|\omega\,f_e^K(\boldsymbol{u}_K^\perp)+\nabla_e^K\,\phi_K\|^2\right]\right]. \quad (13)\end{aligned}$$

Proof. Gathering relations (10) and (11), we obtain the following estimate for the total energy $E_K=\mathcal{P}_K+\mathcal{K}_K$:

$$\begin{aligned}&\frac{\mathrm{d}}{\mathrm{dt}}E_K+\frac{1}{2}\,\mathbf{div}_K^{e,up}\left(\|\boldsymbol{u}_K\|^2\boldsymbol{\mathcal{F}}_e\right)+\phi_K\,\mathrm{div}_K^v(f_v^K(h_K\boldsymbol{u}_K))+h_K\boldsymbol{u}_K\cdot f_K^v\left(\nabla_v^K\,\phi_k\right)\\ &\qquad\le-\omega\left(h_K\boldsymbol{u}_K\cdot f_K^v(f_v^K(\boldsymbol{u}_K^\perp))-\boldsymbol{u}_K\cdot(f_K^e\,\boldsymbol{q}_e)^\perp\right)+\phi_K\,\mathrm{div}_K^e\,\boldsymbol{q}_e\,+\boldsymbol{u}_K\cdot\nabla_K^v\,\pi_v.\end{aligned}$$

By telescoping and using periodic boundary condition we get:

$$\sum_{K\in\mathbb{T}}\mathbf{div}_K^{e,up}\left(\|\boldsymbol{u}_K\|^2\boldsymbol{\mathcal{F}}_e\right)=0.$$

Using iii) of Lemma 3.1 and iv) of Lemma 3.3, we get:

$$\sum_{K\in\mathbb{T}}\left[\phi_K\,\mathrm{div}_K^v(f_v^K(h_K\boldsymbol{u}_K))+h_K\boldsymbol{u}_K\cdot f_K^v\left(\nabla_v^K\,\phi_k\right)\right]=0.$$

Thanks to ii) of Lemma 3.2 we get:

$$\sum_{K\in\mathbb{T}}\left[h_K\boldsymbol{u}_K\cdot f_K^v(f_v^K(\boldsymbol{u}_K^\perp)\right]=0.$$

Finally, i) and ii) of Lemma 3.3 and i) of Lemma 3.2 leads us to the following semi-discrete inequality:

$$\frac{\mathrm{d}}{\mathrm{dt}}\left(\sum_{K\in\mathbb{T}}\Delta x\Delta y E_K\right)\le-\Delta x\Delta y\left[\sum_{v\in\mathbb{V}}\left[\pi_v\,\mathrm{div}_v^K\,\boldsymbol{u}_K\right]+\sum_{e\in\mathbb{E}}\left[\boldsymbol{q}_e\cdot(\omega\,f_e^K(\boldsymbol{u}_K^\perp)+\nabla_e^K\,\phi_K)\right]\right].$$

With the choices (8) and (9), we finally obtain the result. □

Linearized well-balanced property : The linearized version of the scheme (6) is the following:

$$\begin{cases}\dfrac{\mathrm{d}}{\mathrm{dt}}h_K+h_0\;\mathrm{div}_K^v\left(f_v^K\,\boldsymbol{u}_K\right)-h_0\,\mathrm{div}_K^e\,\tilde{\boldsymbol{q}}_e=0,\\ \dfrac{\mathrm{d}}{\mathrm{dt}}\boldsymbol{u}_K+f_K^v(\nabla_v^K\,\phi_K)-\nabla_K^v\,\tilde{\pi}_v=-\omega\left(f_K^v(f_v^K\,\boldsymbol{u}_K)-f_K^e\,\tilde{\boldsymbol{q}}_e\right)^\perp,\end{cases} \quad (14)$$

where

$$\tilde{\boldsymbol{q}}_e=\gamma\,\frac{\Lambda}{gh_0}\max\{\Delta x,\Delta y\}\left(\omega\,f_e^K(\boldsymbol{u}_K^\perp)+\nabla_e^K\,\phi_K\right)\quad\text{and}\quad\tilde{\pi}_v=\nu\Lambda\,\max\{\Delta x,\Delta y\}\,\mathrm{div}_v^K\,\boldsymbol{u}_K.$$

Proposition 4.4. *The linearized scheme* (14) *preserves the discrete geostrophic equilibrium* $\tilde{\boldsymbol{q}}_e = 0$.

Proof. By construction of operators in section 3.2, we get:

$$\omega\, f_v^K(\boldsymbol{u}_K^\perp) + \nabla_v^K\, \phi_K = f_v^e \left(\omega\, f_e^K(\boldsymbol{u}_K^\perp) + \nabla_e^K\, \phi_K\right).$$

Hence, when the geostrophic equilibrium holds on edges, i.e. when $\omega\, f_e^K(\boldsymbol{u}_K^\perp) + \nabla_e^K\, \phi_K = 0$, we get

$$f_K^v(\omega\, f_v^K(\boldsymbol{u}_K^\perp) + \nabla_v^K\, \phi_K) = 0$$

and using property ii) of Lemma 3.1 :

$$\mathrm{div}_v^K\, \boldsymbol{u}_K = -\,\mathrm{div}_v^e((f_e^K(\boldsymbol{u}_K^\perp))^\perp) = \mathrm{div}_v^e\left(\frac{(\nabla_e^K\, \phi_K)^\perp}{\omega}\right).$$

Basic computations then yield $\mathrm{div}_v^K\, \boldsymbol{u}_K = 0$, moreover, using iii) of Lemma 3.1, we get $\mathrm{div}_K^v(f_v^K\, \boldsymbol{u}_K) = 0$. Hence the correction $\tilde{\pi}_v$ equals zero when the geostrophic equilibrium holds on the edges and the scheme (14) preserves this equilibrium. □

Remark 4.5. *As it contains a reconstruction operator on the velocity, the discrete geostrophic equilibrium* $\tilde{\boldsymbol{q}}_e = 0$ *also contains spurious solution*

$$\forall (i,j), \quad \phi_{i,j} = cst \quad and \quad \boldsymbol{u}_{i,j} = \left((-1)^i\, a_j, (-1)^j\, b_i\right)^T.$$

4.2 Other possible 9-point schemes

In the previous section 4.1 we described a scheme which meets our expectations but appears convoluted. In this section, we present two schemes which seem more intuitive, since the flow rate and the perturbation q appear at the same place. In both schemes, the geostrophic equilibrium (3) and the perturbation q are located on edges, whereas the perturbation π is defined on the vertices v. However, none of them succeeds to ensure both the preservation of the linearized stationary states and the decreasing of the nonlinear energy. Nevertheless, the numerical results presented in the last section of the paper exhibit a reasonably good behaviour for all the test cases we have performed.

4.2.1 Solely entropic scheme

In [2], we proposed a first numerical scheme for which we prove that , which is a semi-discrete counterpart of (5). However, we also exhibited the fact that the linearized version of the scheme failed to preserve the geostrophic balance. Using the discrete operators introduced in Section 3.2, this scheme reads :

$$\begin{cases} \dfrac{\mathrm{d}}{\mathrm{dt}} h_K + \mathrm{div}_K^e(\boldsymbol{\mathcal{F}}_e) = 0, \\ \dfrac{\mathrm{d}}{\mathrm{dt}}(h_K \boldsymbol{u}_K) + \mathbf{div}_K^{e,up}(\boldsymbol{u}_K \otimes \boldsymbol{\mathcal{F}}_e) + h_K\; f_K^e(\nabla_e^K\, \phi_K) - \nabla_K^v\, \pi_v = -\omega\,(\,h_K \boldsymbol{u}_K - f_K^e\, \boldsymbol{q}_e)^\perp\,, \end{cases} \tag{15}$$

where the mass fluxes are defined at the level of the edge e as:

$$\boldsymbol{\mathcal{F}}_e = f_e^K(h_K \boldsymbol{u}_K) - \boldsymbol{q}_e\,, \tag{16}$$

with the numerical diffusion term on the flow rate

$$\boldsymbol{q}_e = \gamma\, \frac{\Lambda}{g}\, \max\{\Delta x, \Delta y\}(\omega\, f_e^K(\boldsymbol{u}_K^\perp) + \nabla_e^K\, \phi_K), \tag{17}$$

while the numerical diffusion term on the hydrostatic pressure is defined at the vertices

$$\pi_v = \nu\Lambda\, \max\{\Delta x, \Delta y\}\, f_v^K(h_K)\, \mathrm{div}_v^K(\boldsymbol{u}_K). \tag{18}$$

Decreasing of the semi-discrete energy : We define the total energy as the sum of the potential and kinetic energy : $E_K = \mathcal{P}_K + \mathcal{K}_K$. Then we obtain a discrete counterpart of (5) :

$$\frac{\mathrm{d}}{\mathrm{dt}}\left(\sum_{K\in\mathbb{T}} \Delta x \Delta y E_K\right) \leq -\max\{\Delta x, \Delta y\}\Delta x \Delta y \left(\sum_{e\in\mathcal{E}} \left[\gamma\, \frac{\Lambda}{g} \|\omega\, f_e^K(\boldsymbol{u}_K^\perp) + \nabla_e^K\, \phi_K\|^2\right] + \sum_{v\in\mathbb{V}} \left[\nu\Lambda\, f_v^K(h_K)(\mathrm{div}_v^K\, \boldsymbol{u}_K)^2\right]\right).$$

Proof. Same as Proposition 4.3, using Lemma 3.2 property i) and Lemma 3.3 properties i), ii) and iii). □

Linearized well-balanced property : The numerical diffusion term $\boldsymbol{q}_e \propto \omega\, f_e^K(\boldsymbol{u}_K^\perp) + \nabla_e^K\, \phi_K$ (17) is defined on the edges whereas the geostrophic term $\omega \boldsymbol{u}_K^\perp + f_K^e(\nabla_e^K\, \phi_K)$ that appears in the update of the momentum in (15) is defined on the cells. It is thus obvious that the linearized version of the scheme can not exactly preserve the geostrophic equilibrium. Indeed, if we define the discrete geostrophic equilibrium on the edges, the numerical diffusion term will vanish but not the other one, and vice versa, due to the chosen operators which ensure $f_K^e(f_e^K(\boldsymbol{u}_K^\perp)) \neq \boldsymbol{u}_K^\perp$.

4.2.2 Solely well-balanced scheme

For exhaustiveness, we propose here a slightly modified scheme whose linearized version preserves the geostrophic equilibrium but for which it is not possible to ensure that the semi-discrete energy is non-increasing. This semi-discrete scheme reads :

$$\begin{cases} \dfrac{\mathrm{d}}{\mathrm{dt}} h_K + \mathrm{div}_K^e\, \boldsymbol{\mathcal{F}}_e = 0, \\ \dfrac{\mathrm{d}}{\mathrm{dt}} (h_K \boldsymbol{u}_K) + \mathbf{div}_K^{e,up}(\boldsymbol{u}_K \otimes \boldsymbol{\mathcal{F}}_e) + h_K\, f_K^e(\,\nabla_e^K\, \phi_K) - \nabla_K^v\, \pi_v = -\omega h_K\, f_K^e(f_e^K(\boldsymbol{u}_K^\perp)) + \omega (f_K^e\, \boldsymbol{q}_e)^\perp, \end{cases} \tag{19}$$

with definitions (16), (17) and (18) for the mass flux, the numerical correction on the flow rate and the numerical correction on the pressure term. We see that only the definition of the Coriolis term differs from the previous version.

Linearized well-balanced property : The linearized version of the scheme (19) reads

$$\begin{cases} \dfrac{\mathrm{d}}{\mathrm{dt}} h_K + h_0\ \mathrm{div}_K^e(f_e^K(\boldsymbol{u}_K)) - h_0\, \mathrm{div}_K^e\, \tilde{\boldsymbol{q}}_e = 0, \\ \dfrac{\mathrm{d}}{\mathrm{dt}} \boldsymbol{u}_K + \ f_K^e(\nabla_e^K\, \phi_K) - \ \nabla_K^v\, \tilde{\pi}_v = -\omega\, f_K^e(f_e^K(\boldsymbol{u}_K^\perp)) + \omega (f_K^e\, \tilde{\boldsymbol{q}}_e)^\perp\,, \end{cases} \tag{20}$$

with the numerical diffusion terms

$$\tilde{\boldsymbol{q}}_e = \gamma\, \frac{\Lambda}{g h_0}\, \max\{\Delta x, \Delta y\}\ \left(\omega\, f_e^K(\boldsymbol{u}_K^\perp) + \nabla_e^K\, \phi_K\right) \quad \text{and} \quad \tilde{\pi}_v = \nu \Lambda\ \max\{\Delta x, \Delta y\}\, \mathrm{div}_v^K\, \boldsymbol{u}_K.$$

Proposition 4.6. *Without considering the term* $\mathrm{div}_K^e(f_e^K\, \boldsymbol{u}_K)$*, the linearized scheme* (20) *preserves the discrete geostrophic equilibrium* $\tilde{\boldsymbol{q}}_e = 0$*.*

Proof. When the geostrophic balance expressed on the edges holds, i.e when
$\omega\, f_e^K(\boldsymbol{u}_K^\perp) + \nabla_e^K\, \phi_K = 0$, the geostrophic term that appears in the update of the momentum obviously vanishes

$$f_K^e(\nabla_e^K\, \phi_K) + \omega\, f_K^e(f_e^K(\boldsymbol{u}_K^\perp)) = f_K^e\, \left(\nabla_e^K\, \phi_K + \omega\, f_e^K(\boldsymbol{u}_K^\perp)\right) = 0.$$

Moreover, thanks to Lemma 3.1, we have

$$\mathrm{div}_v^K\, \boldsymbol{u}_K = -\,\mathrm{div}_v^e((f_e^K(\boldsymbol{u}_K^\perp))^\perp) = \mathrm{div}_v^e\, \left(\frac{(\nabla_e^K\, \phi_K)^\perp}{\omega}\right)$$

and obvious computations show that $\mathrm{div}_v^e\, \left((\nabla_e^K\, \phi_K)^\perp\right) = 0$. □

Remark 4.7. *The term* $\mathrm{div}_K^e(f_e^K\, \boldsymbol{u}_K)$ *is not strictly equal to zero when the geostrophic equilibrium holds on the edges of the considered cell. However, by enforcing the geostrophic equilibrium on enough edges of the domain it is possible to write this term on the cell* (i, j) *using solely velocities on cells* $(i \pm 2$ *and/or* $j \pm 2)$*. Due to the complexity of the computations, we failed to prove by recurrence that this term on the cell* (i, j) *can be written using solely velocities on cells* $(i \pm k$ *and/or* $j \pm k)$*, with* k *arbitrarily large. Nevertheless, the test cases presented in Section 5 tend to show that this term is not major and that scheme* (19) *has similar results to other well-balanced scheme. Hence, we assume in the following that scheme* (19) *can be considered as a well-balanced scheme and will be referred to as such.*

Remark 4.8. *As it contains a reconstruction operator on the velocity, the discrete geostrophic equilibrium* $\tilde{\boldsymbol{q}}_e = 0$ *also contains spurious solution*

$$\forall (i,j), \quad \phi_{i,j} = cst \quad and \quad \boldsymbol{u}_{i,j} = \left((-1)^i\ a_j, (-1)^j\ b_i\right)^T.$$

Due to the nonlinear term on the velocity, this spurious solution does not belong to the kernel of the nonlinear scheme (19)*, except when* $a_j = a$ *and* $b_i = b$ *for all* i *and* j*. Numerically, these solutions do not appear in the test cases presented in Section 5. One can note that in the solely entropic scheme* (15)*, there is no reconstruction operator on the velocity and it is difficult to formulate a spurious solution due to the fact that such solution has to verify:*

$$\begin{cases} \omega\, f_e^K(\boldsymbol{u}_K^\perp) + \nabla_e^K\, \phi_K = & 0 \\ \omega \boldsymbol{u}_K^\perp + f_K^e(\nabla_e^K\, \phi_K) = & 0. \end{cases}$$

Numerically, simulations in Section 5 do not show such solutions.

Semi-discrete energy : The computations are similar to the previous scheme but the Coriolis term is no longer the same and some computations show that

$$\langle f_K^e\left(f_e^K(\boldsymbol{u}_K^\perp)\right), \boldsymbol{u}_K\rangle = \frac{1}{2}\sum_{i,j}\left(v_{i,j}\frac{u_{i,j+1}+u_{i,j-1}}{2} - u_{i,j}\frac{v_{i+1,j}+v_{i-1,j}}{2}\right).$$

Hence, there remains a term with no *a priori* sign on the right hand side of the semi-discrete energy inequality. Note that numerical simulations presented in Section 5 tend to show that this term is usually negligible with respect to the non positive correction terms.

4.3 Time discretization

For the discretization in time, fluxes are taken explicit. Nevertheless it is well known - see [8] - that a fully explicit discretization of the Coriolis term leads in that case to unstable schemes. We thus consider the following discretization of the Coriolis term for all the presented schemes:

$$\frac{u_x^{n+1}-u_x^n}{\Delta t} = \omega(\theta_u u_y^n + (1-\theta_u)u_y^{n+1}), \qquad \frac{u_y^{n+1}-u_y^n}{\Delta t} = -\omega(\theta_v u_x^n + (1-\theta_v)u_x^{n+1}),$$

with $\theta_u + \theta_v \leq 1$. Here we choose $\theta_u = 1$ and $\theta_v = 0$ so that the system is solved explicitly. The time step is chosen following [1] such that

$$\Delta t^n \leq \min\left\{\frac{2}{\omega}, \frac{\min(\Delta x, \Delta y)}{\max(\|\boldsymbol{u}^n\| + \sqrt{g h^n})}\right\}.$$

5 Numerical results

In the following, we present different test cases to highlight the comportment of the solely entropic scheme (15), the solely well-balanced scheme (19) and the entropic well-balanced scheme (6), compared to a Godunov-type scheme HLLC. We study the water depth h and the velocity vector field $\boldsymbol{u} = (u, v)$, as well as the energy of the schemes. The numerical experiments are performed with the gravitational constant $g = 1$ and the angular velocity $\omega = 1$. The mesh is defined by a $[101 \times 101]$ Cartesian grid and the numerical diffusion coefficients $\gamma = \nu = 0.5$.

5.1 River test case

This test case is the counterpart of the lake-at-rest for classical shallow water equations. It consist of the simulation of a flow in a stationary state through a channel, with no-slip wall-type boundary condition for $x = -0.5$ and $x = 0.5$, and periodic boundary condition for $y = -0.5$ and $y = 0.5$. The initial condition (see Figure 2) is as follow:

$$\boldsymbol{u} = \begin{pmatrix} 0 \\ \dfrac{\epsilon}{\omega} \end{pmatrix} \quad \text{and} \quad \nabla h = \begin{pmatrix} \dfrac{\epsilon}{g} \\ 0 \end{pmatrix},$$

with $\epsilon = 0.01$.

Hence, this initial condition is both a stationary solution of the nonlinear Shallow Water equations with Coriolis (1) and a geostrophic equilibrium $g \nabla h + \omega \boldsymbol{u}^{\perp} = 0$. We aim at numerical schemes being able to preserve this solution.

In Figures 4a and 4b, the proposed scheme (6) exactly preserves the initial condition. Due to the wall-type boundary condition the solely entropic scheme (15) presents some anomalies on the wall boundaries on both the water depth and the velocities, as does the solely well-balanced scheme (19) but only on the water depth. Apart from theses defaults, the schemes preserve the stationary solution. Finally, the HLLC scheme do not preserve the initial condition and will tend to the lake-at-rest state.

In Figure 3 the energy fully discrete is preserved by our schemes, whereas it is decreasing for HLLC scheme.

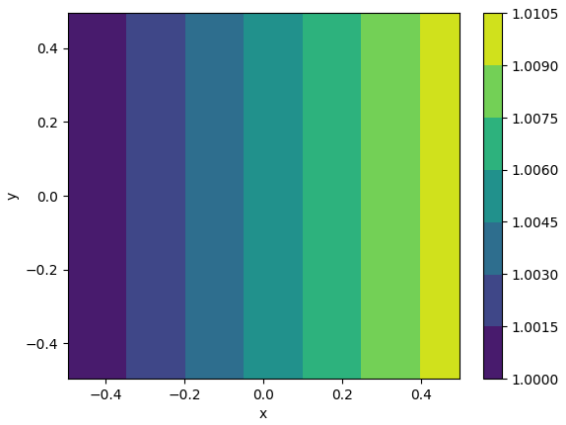

Figure 2: Initial water depth.

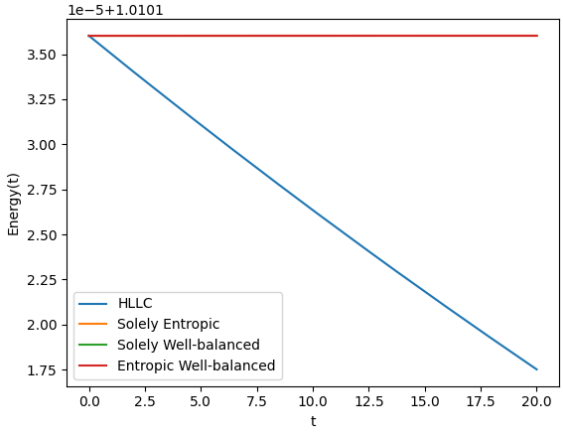

Figure 3: Energy of the system in function of time.

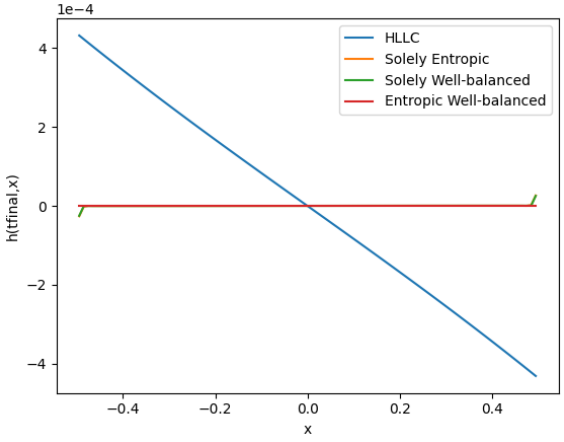

(a) Difference on Water depth

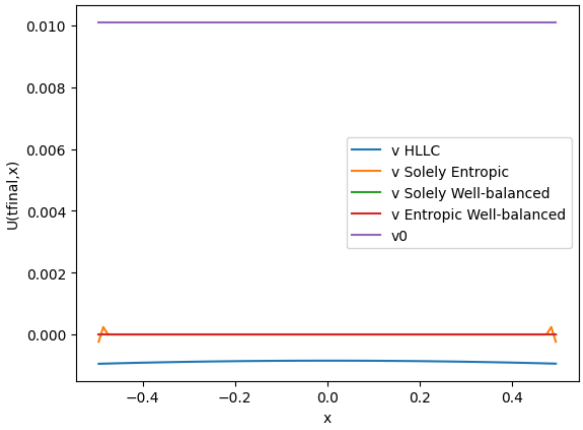

(b) Difference on Velocity v

Figure 4: Cross section in $y = 0$ of solution at $t = 20s$ difference to initial state.

5.2 Stationary vortex test case

We consider the test case introduced in [3] and defined by :

$$h(r) = \begin{cases} 1 + \dfrac{5\omega\epsilon}{2g} r^2 \text{ if } r \leqslant 0.2 \\ 1 + \dfrac{\omega\epsilon}{10g} - \dfrac{\omega\epsilon}{g}(0.3 - 2r + 2.5r^2) + \dfrac{\epsilon^2}{g}(3.5 - 20r + 12.5r^2 + 4\ln(5r)) \text{ if } 0.2 < r \leqslant 0.4 \\ 1 + \dfrac{\omega\epsilon}{5g} + \dfrac{\epsilon^2}{g}(4\ln(2) - 2.5) \text{ if } r > 0.4 \end{cases}$$

$$\text{and} \quad \boldsymbol{u}(r,\theta) = \begin{cases} -5\epsilon\ r\ {}^t(\sin(\theta),\cos(\theta)) \text{ if } r \leqslant 0.2 \\ -(2-5r)\epsilon\ {}^t(\sin(\theta),\cos(\theta)) \text{ if } 0.2 < r \leqslant 0.4 \\ 0 \text{ if } r > 0.4 \end{cases}$$

where r and θ are the polar coordinates of a point of the domain. The parameter ϵ influences the initial water velocity of the vortex, which is linked to the gradient of the water depth through the geostrophic equilibrium. This create a stationary vortex that is a stationary solution of the nonlinear Shallow Water equations with Coriolis (1). Let us recall that this stationary solution is different from the geostrophic equilibrium (3) since the definition of the water depth contains a second term that is related to the nonlinear advective term in the equations. Nevertheless, when the coefficient ϵ introduced in the definition of the velocity field is small, the nonlinear term in the definition of the water depth is much smaller than the linear term and the stationary solution is very close to a geostrophic equilibrium. This initial condition can be seen on Figure 5. Finally, the domain has periodic boundary conditions.

We take $\epsilon = 0.01$ and a final simulation time of $200s$. For this test case, the solely entropic, solely well-balanced and entropic well-balanced schemes all give similar results except the solely entropic one which slightly stand out. We thus choose to showcase only one scheme on the 2D graphs, the entropic well-balanced one.

After $200s$, on Figures 6, 7 and 8 we can notice that our three schemes indeed mainly preserves the vortex. In that amount of time, the velocities and the depth of the vortex slightly reduced, but the overall shape of the vertex is preserved. Meanwhile, we can see that the HLLC scheme failed to preserve the said shape : the velocities and the depth reduced greatly, qualitatively, stratified velocity can be seen on Figure 7 whereas a distorted vortex appears on Figure 6 hence the scheme seems to try to reach a lake at rest state.

In order to quantity the preservation of the stationary vortex, we introduce the following relative error:

$$\frac{|\min(h_{final}) - \min(h_{init})|}{\max(h_{init}) - \min(h_{init})},$$

which track the bottom of the vortex. On Figure 9, we remark that the HLLC scheme quickly move away from the vortex, we can also note that the final water depth relative error made by our schemes decreases with ϵ, while this parameter has no influence on the error for the HLLC scheme. Indeed, for any value of ϵ, the HLLC scheme has the same behaviour : the stationary vortex is not seen as an equilibrium and the difference of initial state thus has no effect while the scheme tries to reach the closest equilibrium in its kernel, the lake at rest. Meanwhile, the schemes developed previously do consider the stationary vortex as a geostrophic equilibrium even if it is not a stationary solution for the scheme. Thus, when ϵ decrease the non-linear term in the schemes become negligible and the vortex appears as a quasi-equilibrium for the scheme.

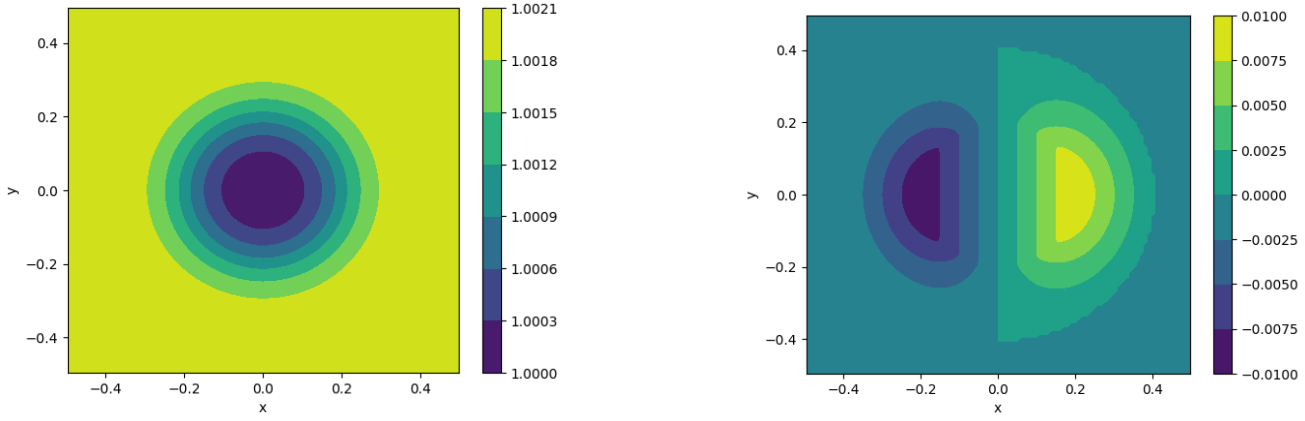

(a) Water depth

(b) Velocity v

Figure 5: Initial state of the stationary vortex.

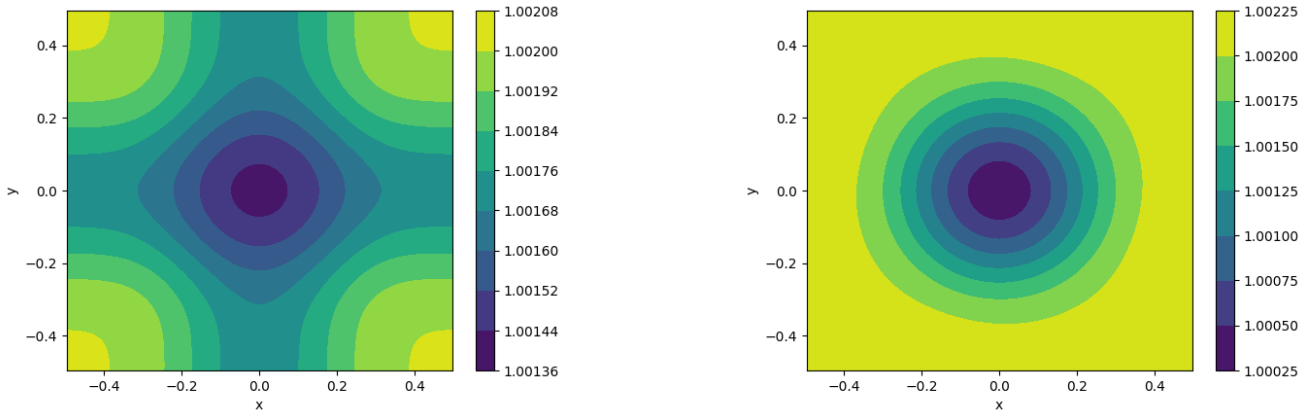

(a) HLLC scheme

(b) Entropic well-balanced scheme

Figure 6: Water depth at $t = 200s$.

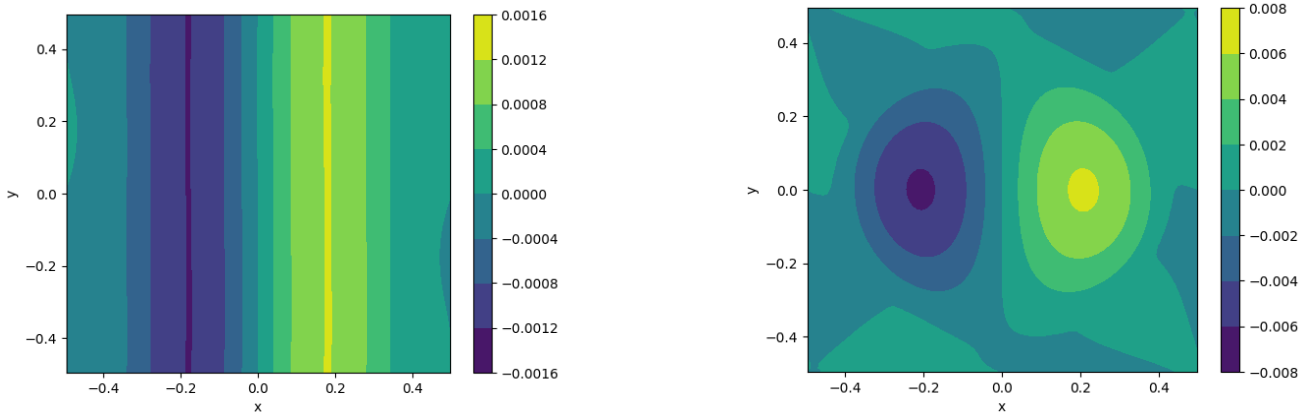

(a) HLLC scheme

(b) Entropic well-balanced scheme

Figure 7: Velocity v at $t = 200s$.

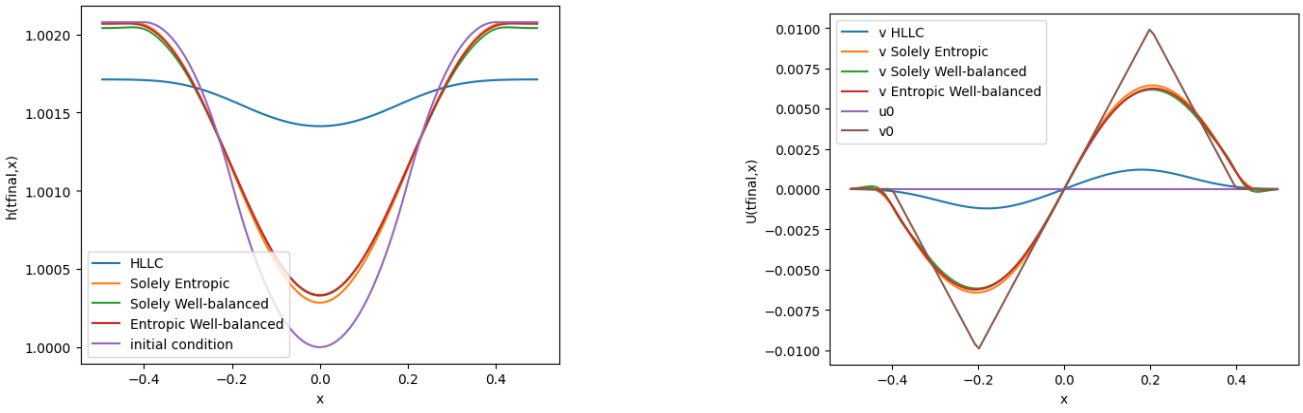

(a) Water depth

(b) Velocity v

Figure 8: Cross sections $y = 0$ of solution at $t = 200s$.

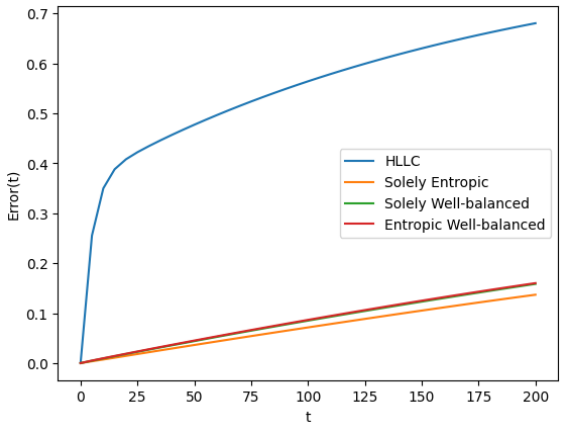

(a) For the different scheme in function of time

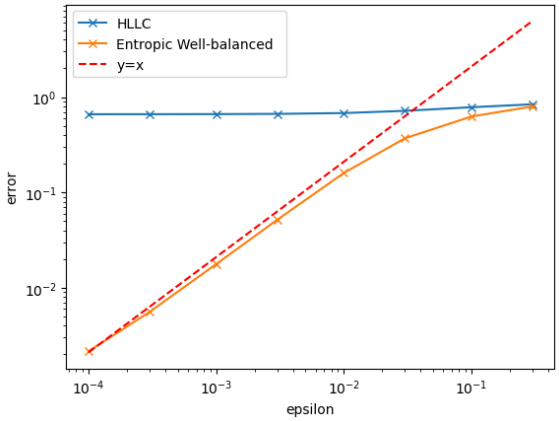

(b) For the different ϵ at $t = 200s$

Figure 9: Water depth relative error to initial state.

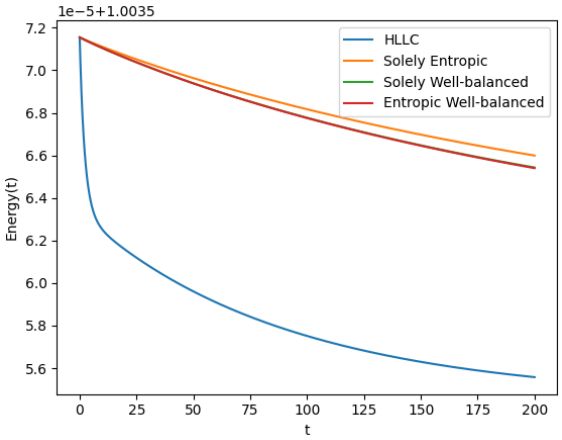

Figure 10: Energy of the system in function of time for $\epsilon = 0.01$.

5.3 Translated vortex test case

This test case is the sum of two other ones : the river and the linear stationary vortex. Both are stationary solutions of the linear Shallow Water equations with Coriolis source term, and we are interested in the behaviour of the presented schemes when given that initial state (see Figure 11). As for the river test case, we enforce wall-type boundary condition for $x = -0.5$ and $x = 0.5$, and periodic boundary condition for $y = -0.5$ and $y = 0.5$. The slope of the river is $\epsilon = 0.01$, same as the vortex depth parameter.

After 20 seconds, we find in Figures 12 , 13 and 14 that the HLLC-scheme fails to preserve the initial state : the vortex is flattening out and the slope is decreasing. After 500s, it is brought back to the lake-at-rest equilibrium. The other schemes also have a behaviour on par with the one they had on the two previous test cases and their graphs are overlapped. The vortex is preserved, except for a small depth reduction, and the slope of the river is constant. In addition, the river induces a translation of the vortex along the y axis.

On Figure 16, we can note that the energy is also what one could expect from this superposition of solution : it is almost constant for the presented schemes, while it drops abruptly for the HLLC one.

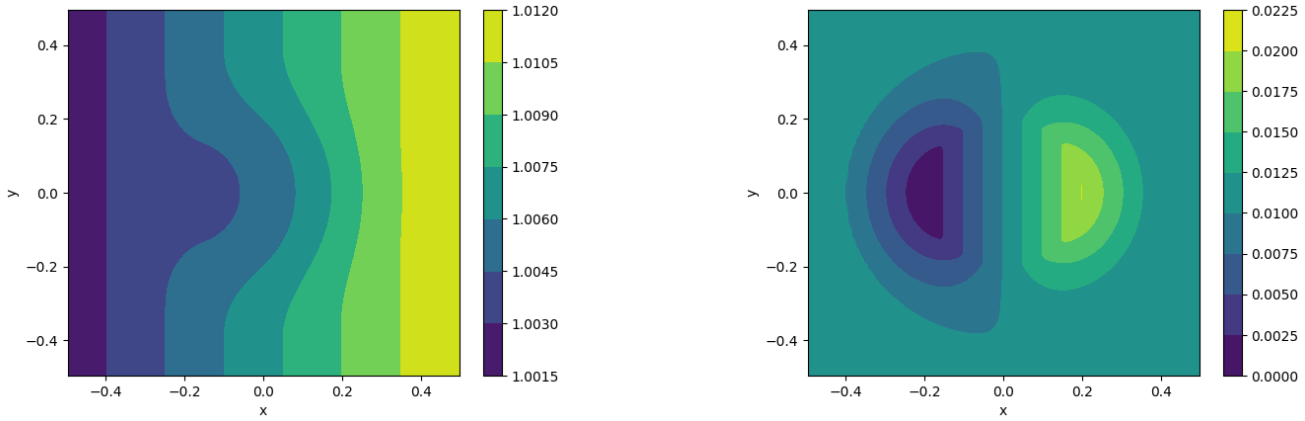

(a) Water depth

(b) Velocity v

Figure 11: Initial state of the translated vortex.

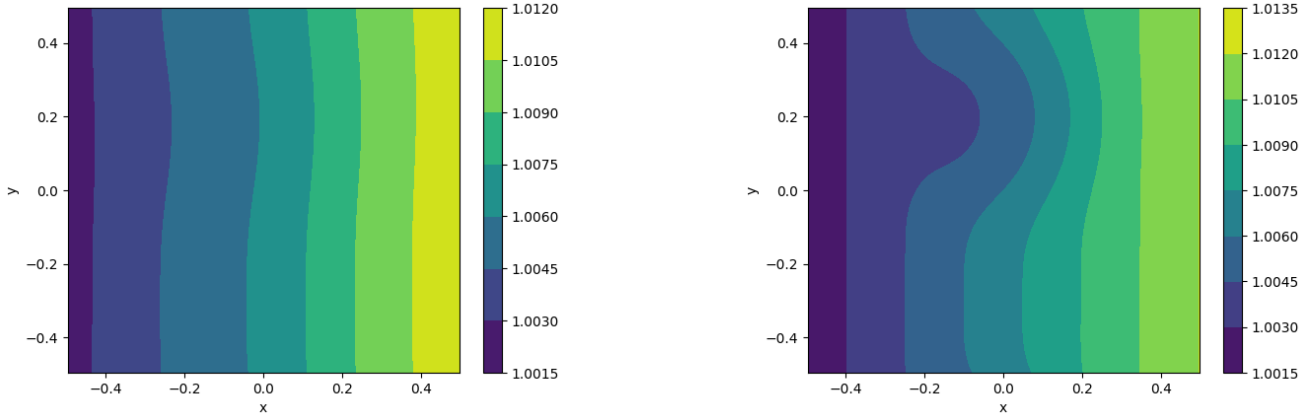

(a) HLLC scheme

(b) Entropic Well-balanced scheme

Figure 12: Water depth at $t = 20s$.

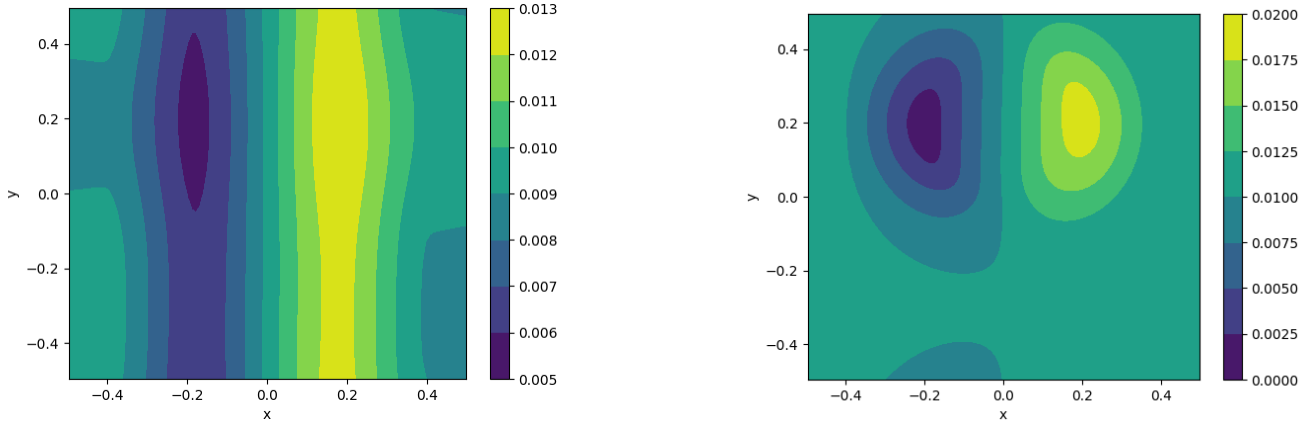

(a) HLLC scheme

(b) Entropic Well-balanced scheme

Figure 13: Velocity v at $t = 20s$.

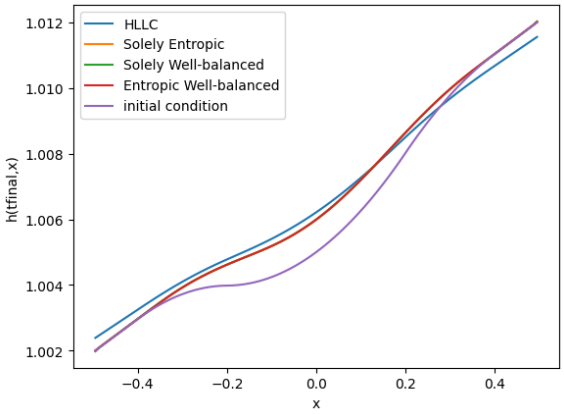

(a) $x = 0$ cross section

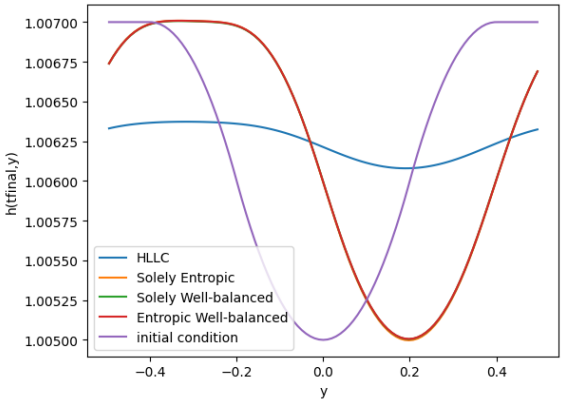

(b) $y = 0$ cross section

Figure 14: Cross section of water depth at $t = 20s$ in $x = 0$ (a) and $y = 0$ (b).

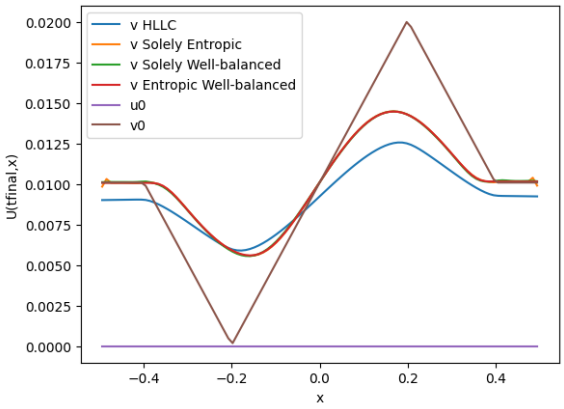

(a) $x = 0$ cross section

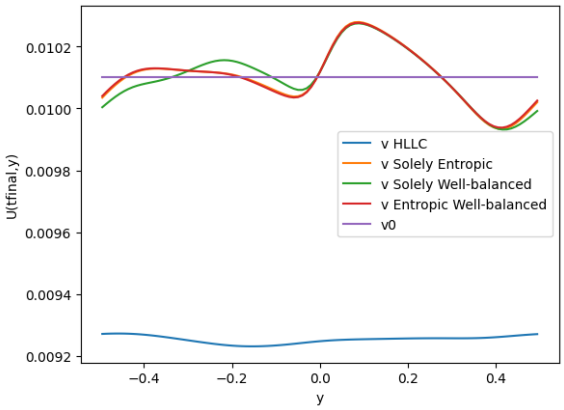

(b) $y = 0$ cross section

Figure 15: Cross section of velocity v at $t = 20s$ in $x = 0$ (a) and $y = 0$ (b).

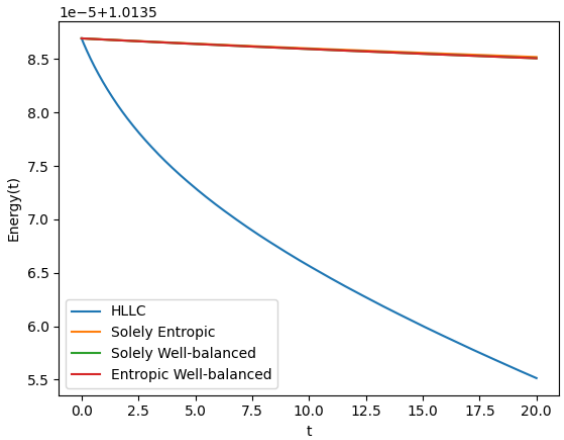

Figure 16: Energy of the system in function of time for the different schemes.

5.4 Water-column test case

We consider a circular dam break with a radius of 1 and the domain has periodic boundary conditions. At $t = 0$, the velocity is zero throughout the domain and and the water height is 1 except for a water column in the center of height 2.

This initial condition is very far from a geostrophic equilibrium, thus on Figure 20 we can see that the energy drop is sharper than previously. The schemes have similar energy, except that the solely entropic scheme drops a little lower, while the graphs of the entropic well-balanced and solely well-balanced are overlapped.

On Figure 19, we notice that all schemes have the same overall behaviour at the beginning. However, at time goes by, a change is noticeable as the HLLC-scheme gets to a lake at rest equilibrium, while the presented schemes stabilize around another geostrophic equilibrium. Except at $t = 1s$, the graphs of the entropic well-balanced and solely well balanced schemes are overlapped.

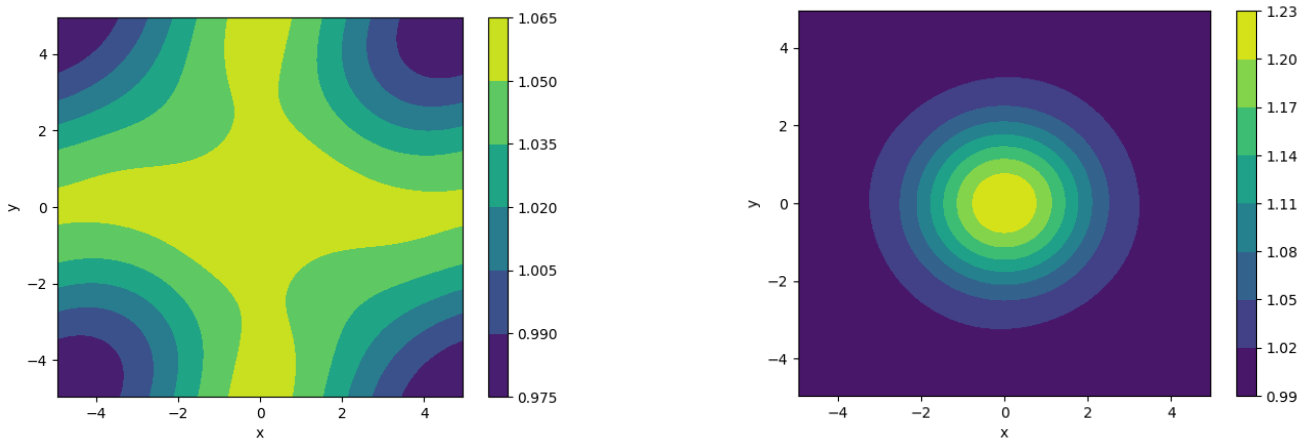

(a) HLLC scheme

(b) Entropic Well-balanced scheme

Figure 17: Water depth at $t = 100s$.

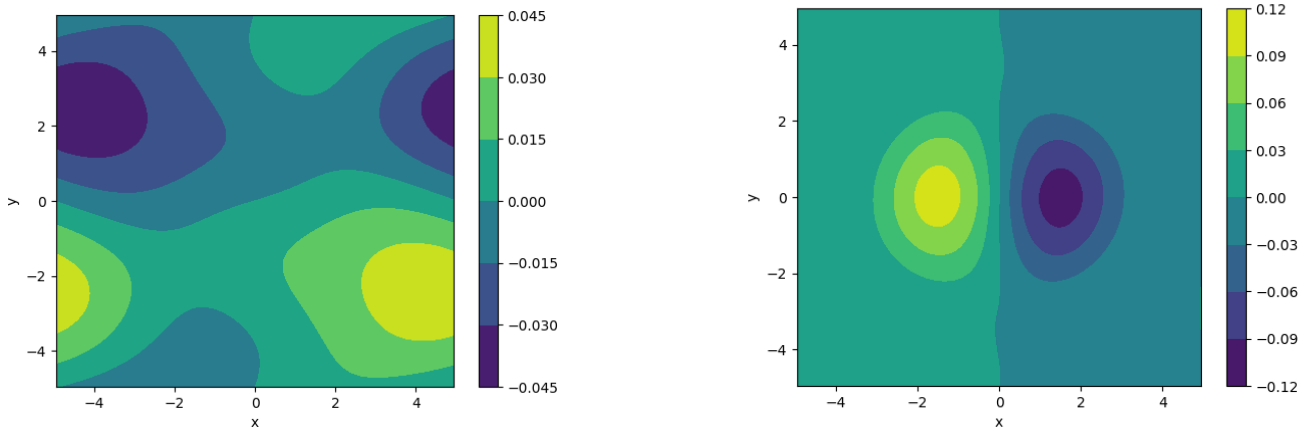

(a) HLLC scheme

(b) Entropic Well-balanced scheme

Figure 18: Velocity v at $t = 100s$.

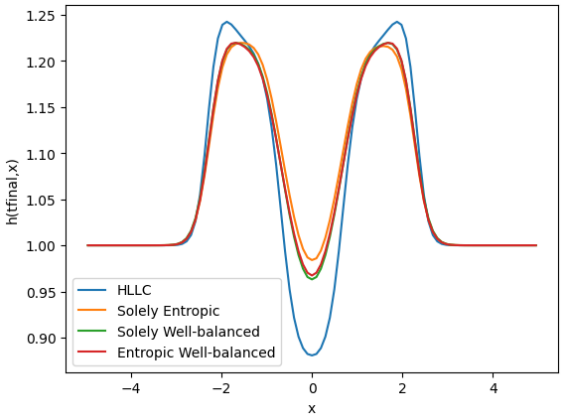

(a) $t = 1s$

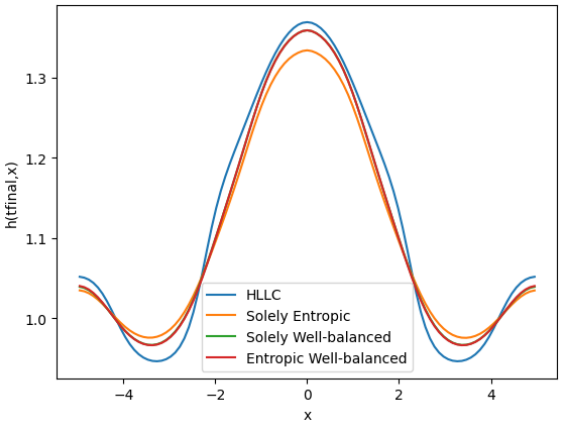

(b) $t = 4s$

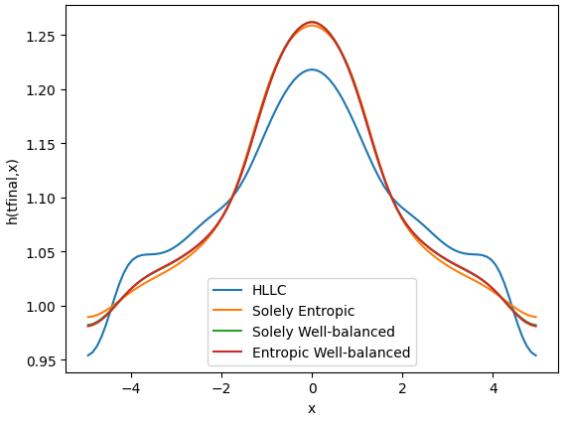

(c) $t = 6s$

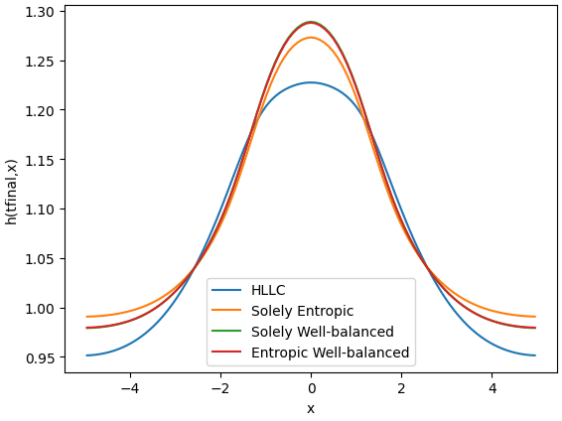

(d) $t = 10s$

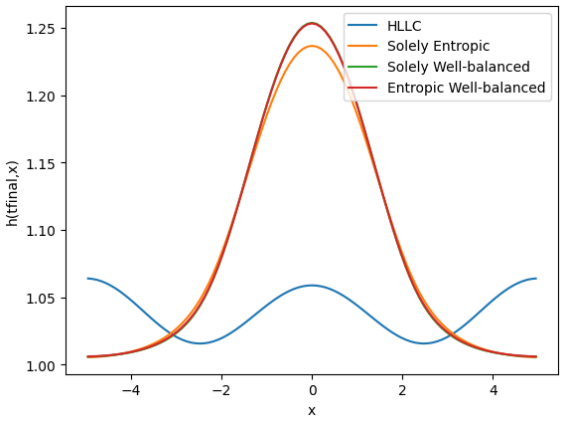

(e) $t = 40s$

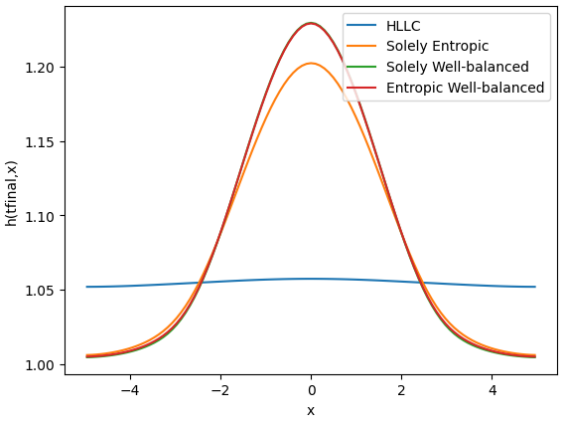

(f) $t = 100s$

Figure 19: Cross section in $y = 0$ of simulation results for the different schemes at different times.

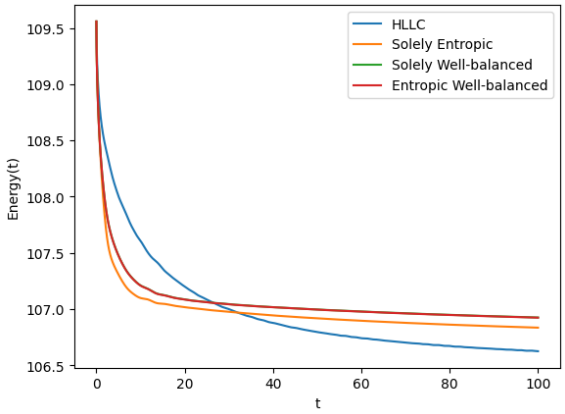

Figure 20: Energy of the system in function of time for the different schemes.

5.5 Instabilities of the solely well-balanced scheme

We want to showcase here the instabilities that can appear with the solely well-balanced scheme. It is a variation on the water column test case, where the height of the column is $\epsilon = 0.01$ and the simulation is left running for $200s$. We can notice on Figure 21 that the entropic well-balanced and solely entropic scheme show no sign of instability, while bother the water depth and the velocities of solely well-balanced scheme became erratic. As for the energy on Figure 22, the solely entropic and entropic well-balanced have the expected behavior, while the energy of the solely well-balanced spikes after $150s$.

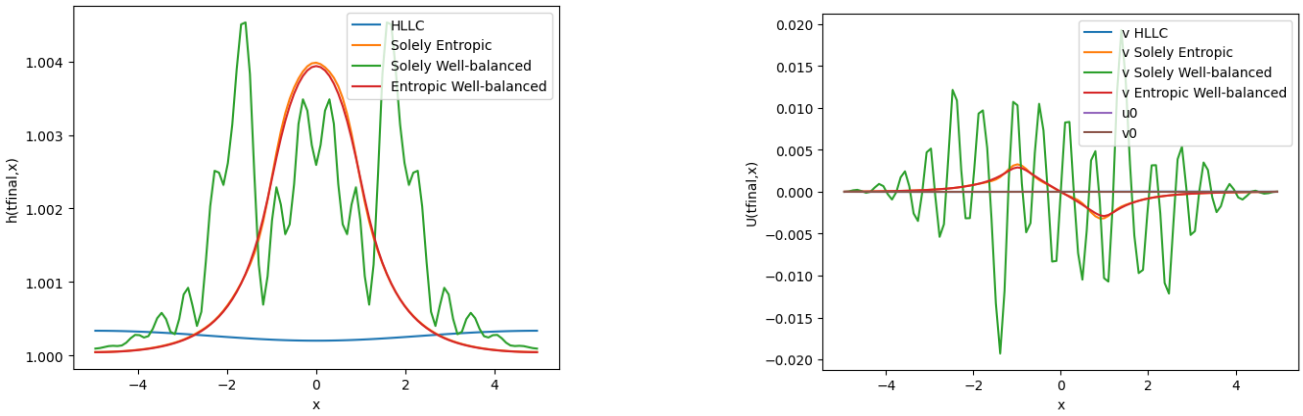

(a) Water depth

(b) Velocity v

Figure 21: Cross sections $y = 0$ of solution at $t = 200s$.

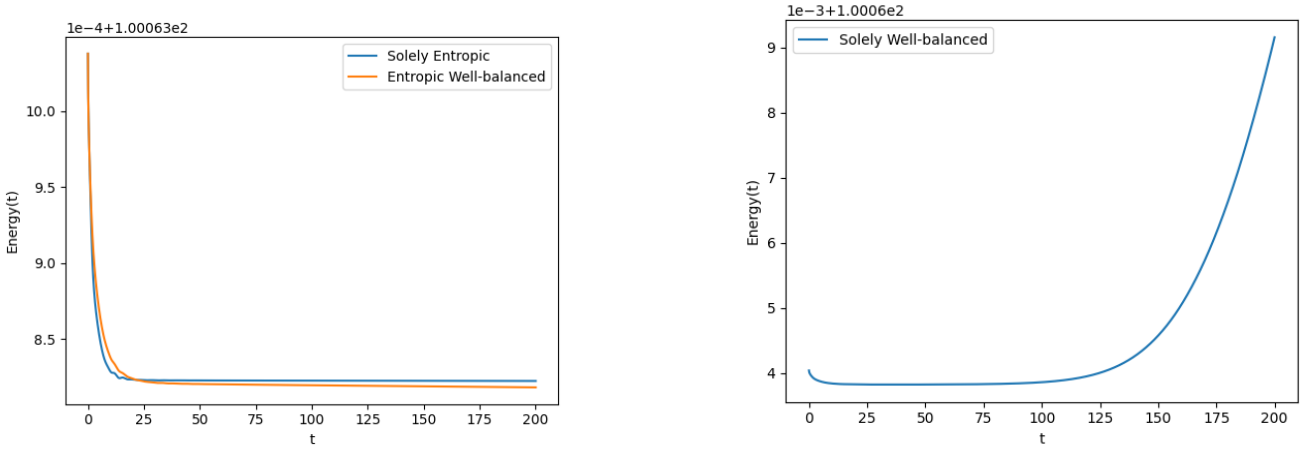

(a) Edge-based entropic et Edge-Vertex

(b) Edge-based WB

Figure 22: Energy of the system in function of time for the different schemes.

6 Conclusion

In this work we have derived three semi-discrete schemes, namely solely entropic, solely well-balanced and entropic well-balanced for the shallow water equations with Coriolis force.

For the solely entropic scheme, the geostrophic equilibrium in the momentum balance equation is discretized on the cells of the mesh and discretized on the edges in one of the perturbation. This choice ensure a non-increasing energy for the semi-discrete scheme while the linearly well-balanced property cannot be achieved. However, these two discretizations of geostrophic equilibrium are close enough to allow the scheme to be more accurate than the HLLC one around the geostrophic equilibrium.

For the solely well-balanced scheme, the geostrophic equilibrium is only discretized on the edges of the mesh and thus the linearly semi-discrete scheme is well-balanced. Although we failed to ensure the non-increasing energy, the numerical tests show a good short-term behaviour.

For the entropic well-balanced scheme, the geostrophic equilibrium in the momentum balance equation is discretized on the vertices of the mesh, except in one of the perturbation where it is discretized on the edges. The linearly semi-discrete scheme is well-balanced and we have semi-discrete energy estimate. Furthermore, the stencil is kept compact and spurious solutions do not appear in the presented test case.

Future works will be dedicated to the study of the fully discrete energy of the schemes and to the extension of the strategy to triangular meshes through more realistic test cases.

References

[1] E. Audusse, M. Do, P. Omnes, and Y. Penel. Analysis of modified godunov type schemes for the two-dimensional linear wave equation with coriolis source term on cartesian meshes. *Journal of Computational Physics*, 373:91–129, 2018.

[2] E. Audusse, V. Dubos, A. Duran, N. Gaveau, Y. Nasseri, and Y. Penel. Numerical approximation of the shallow water equations with Coriolis source term. *ESAIM: Proceedings*, 70:31–44, June 2021.

[3] E. Audusse, R. Klein, and A. Owinoh. Conservative discretization of coriolis force in a finite volume framework. *Journal of Computational Physics*, 228(8):2934–2950, 2009.

[4] A. Bermudez and M. Vazquez-Cendon. Upwind Methods for Hyperbolic Conservation Laws with Source Terms. *Computers and Fluids*, 23(8):1049–1071, 1994.

[5] C. Berthon, M. M'Baye, M. H. Le, and D. Seck. A well-defined moving steady states capturing Godunov-type scheme for Shallow-water model. *International Journal on Finite Volumes*, 15, 2020.

[6] F. Bouchut. *Nonlinear stability of finite volume methods for hyperbolic conservation laws, and well-balanced schemes for sources*, volume 2/2004. Birkhäuser Basel, 2004.

[7] F. Bouchut, J. Le Sommer, and V. Zeitlin. Frontal geostrophic adjustment and nonlinear wave phenomena in one-dimensional rotating shallow water. Part 2. High-resolution numerical simulations. *Journal of Fluid Mechanics*, 514:35–63, 2004.

[8] M. Castro, J. Antonio López, and C. Pares. Finite volume simulation of the geostrophic adjustment in a rotating shallow-water system. *SIAM Journal on Scientific Computing*, 31:444–477, 01 2008.

[9] A. Chertock, M. Dudzinski, A. Kurganov, and M. Lukácová-Medvid'ová. Well-balanced schemes for the shallow water equations with coriolis forces. *Numerische Mathematik*, 138:939–973, 2018.

[10] F. Couderc, A. Duran, and J.-P. Vila. An explicit asymptotic preserving low froude scheme for the multilayer shallow water model with density stratification. *Journal of Computational Physics*, 343:235–270, 2017.

[11] J. R. Edwards. Reflections on the early development of the "ausm family" of riemann solvers. *Shock Waves*, 29(5):601–609, 2019.

[12] R. Eymard, T. Gallouët, and R. Herbin. *Finite Volume Methods*, volume 7 of *Handbook of Numerical Analysis*. Elsevier, 2000.

[13] L. Gosse. *Computing qualitatively correct approximations of balance laws*, volume 2. Springer, 2013.

[14] J. Greenberg and A. LeRoux. A well-balanced scheme for the numerical processing of source terms in hyperbolic equations. *SIAM Journal on Numerical Analysis*, 33(1):1–16, 1996.

[15] S. Jin. Efficient asymptotic-preserving (AP) schemes for some multiscale kinetic equations. *SIAM Journal on Scientific Computing*, 21(2):441–454, 1999.

[16] R. J. LeVeque. *Finite volume methods for hyperbolic problems*. Cambridge Texts in Applied Mathematics. Cambridge University Press, Cambridge, 2002.

[17] M.-S. Liou. A sequel to ausm: Ausm+. *Journal of Computational Physics*, 129(2):364–382, 1996.

[18] M.-S. Liou and C. J. Steffen. A new flux splitting scheme. *Journal of Computational Physics*, 107(1):23–39, 1993.

[19] X. Liu, A. Chertock, and A. Kurganov. An asymptotic preserving scheme for the two-dimensional shallow water equations with Coriolis forces. *Journal of Computational Physics*, 391:259–279, 2019.

[20] M. Parisot and J.-P. Vila. Centered-potential regularization for the advection upstream splitting method. *SIAM Journal on Numerical Analysis*, 54(5):3083–3104, 2015.

[21] T. Ringler, J. Thuburn, J. Klemp, and W. Skamarock. A unified approach to energy conservation and potential vorticity dynamics for arbitrarily-structured c-grids. *Journal of Computational Physics*, 229(9):3065–3090, 2010.

[22] J. Thuburn, T. Ringler, W. Skamarock, and J. Klemp. Numerical representation of geostrophic modes on arbitrarily structured c-grids. *Journal of Computational Physics*, 228(22):8321–8335, 2009.

[23] E. F. Toro. *Riemann Solvers and Numerical Methods for Fluid Dynamics*. Springer, 2009.

[24] R. A. Walters, E. Hanert, J. Pietrzak, and D. Le Roux. Comparison of unstructured, staggered grid methods for the shallow water equations. *Ocean Modelling*, 28(1):106–117, 2009. The Sixth International Workshop on Unstructured Mesh Numerical Modelling of Coastal, Shelf and Ocean Flows.

[25] R. A. Walters, E. M. Lane, and E. Hanert. Useful time-stepping methods for the coriolis term in a shallow water model. *Ocean Modelling*, 28(1):66–74, 2009. The Sixth International Workshop on Unstructured Mesh Numerical Modelling of Coastal, Shelf and Ocean Flows.

[26] H. Zakerzadeh. The rs-imex scheme for the rotating shallow water equations with the coriolis force. In C. Cances and P. Omnes, editors, *Finite Volumes for Complex Applications VIII - Methods and Theoretical Aspects*, pages 199–207. Springer, 2017.

[27] V. Zeitlin. *Geophysical fluid dynamics: understanding (almost) everything with rotating shallow water models*. Oxford University Press, 2018.